https://dx.doi.org/10.4314/ijs.v26i1.10

LITHOLOGICAL DISCRIMINATION AND MAPPING IN PART OF THE UPPER BENUE TROUGH USING LANDSAT 8

Abodunrin, O. A., Fagbohun, B. J.* and Anifowose, A. Y. B.
Department of Remote Sensing and Geoscience Information System, Federal University of Technology, Akure, Nigeria.
*Corresponding Author's Email: bjfagbohun@futa.edu.ng
(Received: 18th July, 2023; Accepted: 27th March, 2024)

ABSTRACT

This study focused on evaluating the efficiency and complementarity of image enhancement techniques for lithological discrimination and mapping in the upper parts of Benue Trough using Landsat 8 data. To achieve this, image enhancement techniques such optimum index factor, band ratio, principal component analysis, and minimum noise fraction were applied on Landsat 8 OLI data covering parts of the Upper Benue Trough. False colour composites (FCC) were created from three most informative derivatives of these image enhancements. The FCCs were compared in terms of their capability to differentiate different lithological units in the study area by comparing the FCCs with existing geological map. The results show that the FCC created from band ratios provided the highest amount of information, while those created based on optimum index factor provided the least amount of information with respect to lithological discrimination. Additionally, it was observed that the FCCs created from the derivatives of band ratio, principal component analysis and minimum noise fraction provide complementarity. Thus, the three FCCs from these three enhancement methods were fused into a single image, which further aided lithological discrimination. By combining the outputs from three image enhancement techniques, most of the sedimentary and crystalline rocks in the study area were successfully delineated. The method adopted in this study particularly the fusion of outputs from band ratio, principal component analysis and minimum noise fraction represents a novel approach that is suitable for lithological mapping in remote areas, particularly arid and semi-arid terrains with considerable rock exposure.

Keywords: Remote sensing, Upper Benue, Lithological mapping, Principal component analysis, Band ratio, Minimum noise fraction.

INTRODUCTION

Remote sensing has evolved as a reconnaissance mapping tool for geoscientists due to its ability to cover large areas and provide desirable information in a shorter time frame compared to traditional field mapping (Gupta, 1981, Drury, 1987; van der Meer *et al.*, 2012; Hardlar, 2013). Improvement in the capabilities of sensors has expanded the geological applications of remote sensing to terranes that cannot be easily accessed (Lopes *et al.*, 2016; Pour *et al.*, 2017). Remote sensing offers the possibility to overcome the difficulties and limitations associated with lithological mapping by providing synoptic view of inaccessible geologic terranes that are of interest (Lopes *et al.*, 2016; Mohamed *et al.*, 2021).

With the availability of several satellite images from various sensors, satellite remote sensing has gradually replaced aerial photos for most geological applications. Modern day satellites provide geoscientists with significant amount of information on mineralogical composition of rocks on the earth surface, enabling successful applications in both lithological and alteration mapping (Abrams *et al.*, 1983; Sultan *et al.*, 1986; Kaufmann, 1988; Sabins, 1999; Carranza and Hale, 2002; Hassan *et al.*, 2017; van der Meer *et al.*, 2012; Rowan *et al.*, 1977; Gad and Kusky, 2002; Rajendran *et al.*, 2011; Kumar *et al.*, 2015; Ibrahim *et al.*, 2016; Fagbohun *et al.*, 2017; Abdelmalik and Abd-Allah, 2017; Hewson *et al.*, 2017; Mahanta and Maiti, 2018; El-Din and Abdelkareem, 2018; Zoheir *et al.*, 2019; El Janati, 2019; Peyghambari and Zhang, 2021; Suliman *et al.*, 2023; Courba *et al.*, 2023).

Initial use of remote sensing images for lithological mapping were focused on the use of black and white analogue aerial photos, followed by coloured photos. On this type images, tone/colour, pattern and textural characteristics of the lithologies aided the identification and discrimination of lithologies (Drury, 1987). With the advent of satellite-based multispectral sensors, digital images with several bands outside the visible region of the electromagnetic spectrum became available. This enabled the creation of

many colour composites apart from the true colour composite, which further aided lithological interpretation and discrimination. Nevertheless, the presence of high correlation among contiguous image bands, introduced another limitation in the use of colour composites for lithological mapping.

The advancements in computer technology particularly in the area of computer vision and digital image processing further improved the amount of geological information that can be derived from remotely sensed data. Image processing and enhancement methods that subdue the correlation between image bands such as Band Ratioing (BR), Principal Component Analysis (PCA), and Minimum Noise Fraction (MNF) were developed for mineralogical and lithological mapping using remotely sensed images (Abrams, 1983; Sultan *et al*., 1986, van der Meer *et al*., 2012; Bentahar and Raji, 2021, Fahmy *et al*., 2023; Courba *et al*., 2023). These methods are particularly useful for lithological discrimination where there are rocks with slight variation in mineralogical compositions. The outputs from these enhancement techniques are usually visualized as false colour composites (FCC) to enable lithological discrimination and mapping (Fahmy *et al*., 2023). While the FCC from each of these enhancement methods are usually sufficient to discriminate many lithologies, in some cases, each enhancement method tends to effectively discriminate different rock types (Fagbohun *et al*., 2017). Thus, these image enhancements are often used together in order to achieve the best results in terms of lithological discrimination and mapping. This is mostly done visually and few studies have explored the idea of fusing the outputs from two or more enhancement methods to improve the utility of the outputs of these image enhancement (Pour and Hashim, 2013; Mahanta and Maiti, 2018; Xi *et al*., 2022).

The Upper Benue is located in northeastern part of Nigeria where field survey can be challenging. Advanced analysis and enhancements of remotely sensed data for lithological mapping presents a reliable approach to improve existing geological map in the area. A number of studies have been carried out in the Benue Trough involving the use remote sensing (Isiorho, 1989; Okereke *et al*., 2012, Idi and Aliyu, 2015; Onum *et al*., 2021). However, most of these studies are focused on structural and geodynamic mapping as well as alteration mineral mapping (Idi and Aliyu, 2015; Onum *et al*., 2021). The application of remote sensing for lithological mapping in the Benue Trough particularly Upper Benue is limited. More so, the application of image enhancement techniques such as BR, PCA, and MNF, and the combination of the outputs from these techniques for lithological mapping in the Upper Benue Trough has not yet be carried out. Thus, this study is focused on comparison and integration of image enhancement techniques for lithological discrimination and mapping in the upper part of Benue Trough.

THE STUDY AREA

The study area is located in northeastern part of Nigeria within the Gongola arm of the Upper Benue Trough (Figure 1a), which is considered a failed arm of a triple junction (Burke and Dewey, 1973; Olade, 1975). Because the area located in the semi-arid region, it is devoid of thick vegetation cover, and therefore has considerable rock exposure. The area is underlain by porphyroblastic gneiss of Precambrian age, which is intruded by Older Granite during the Pan African event. Other rock types in the area include feldspathic sandstone and shelly limestone deposited during the Albian; shale, limestone and sandstone; black shale, siltstone and sandstone; clay, grit and pebbles deposited during the Turonian; sands, clays, siltstone and limestone deposited during the Cenomanian; and Tertiary basalts that intrude the sedimentary sequence (Figure 1b).

Geological Setting of the Benue Trough

The Benue Trough is an approximately 1000 km elongated structure, extending from the Atlantic coast of Nigeria to Chad Basin in the northeastern part of Nigeria (Benkhelil, 1989; Ofoegbu, 1985). The Trough is divided into the Upper Benue located in the northeastern part of Nigeria, Middle Benue located in the Central part of Nigeria and Lower Benue in the Southern part of Nigeria. The Benue Trough evolved as a result of rift faulting and folding of the basement during the continental rifting event that separated the African and South American plates during the Cretaceous (Cartel *et al*., 1963). The subsidence

along the Benue Trough, which is bounded by crystalline basement (the North Central and West African Shield to the west, and Adamawa highland to the east) started around mid-Albian and continued until late Senonian. The oldest rocks in the Benue Trough are the Basement Complex rocks comprising of quartzo-feldspathic magmatite-gneisses with occasional quartzites, marbles and amphibolites. These Basement rocks, which are sparsely exposed within the Trough are intruded by Pan African granitoids and some minor intrusives (Ofoegbu, 1985).

During the Cretaceous, sediments with ages ranging from Middle Albian to Maastrichtian were deposited in the Trough (Wright, 1985). In the Upper Benue where the study area belongs, the Yola and Bima fluvio-deltaic sandstones deposited during Albian to Cenomanian are the oldest sediments. The cross-bedded conglomeratic sandstones at the bottom of the sequence, have some lenses of clay and shale (Wright, 1985). Marine shales and sandstones of Yolde Formation deposited during the Turonian overlie the Albian sandstones. The Yolde Formation grades into a sequence of shales interlayered with thin nodular limestones and some sandstones of the Pindiga Formation. North of the Zambuk Ridge, the Pindiga Formation graduates into Gongila Formation and Fika shales, a sequence comprising limestone, sandstone and shales. The Gombe Sandstone, which is a flaggy cross-bedded sandstone interbedded with ironstones is also found north of Zambuk Ridge, where it is unconformably overlain by Kerrikerri Formation, a fluviatile and lacustrine sequence consisting of reddish sandstones, clays, grits and thin layers of conglomerates (Wright, 1985).

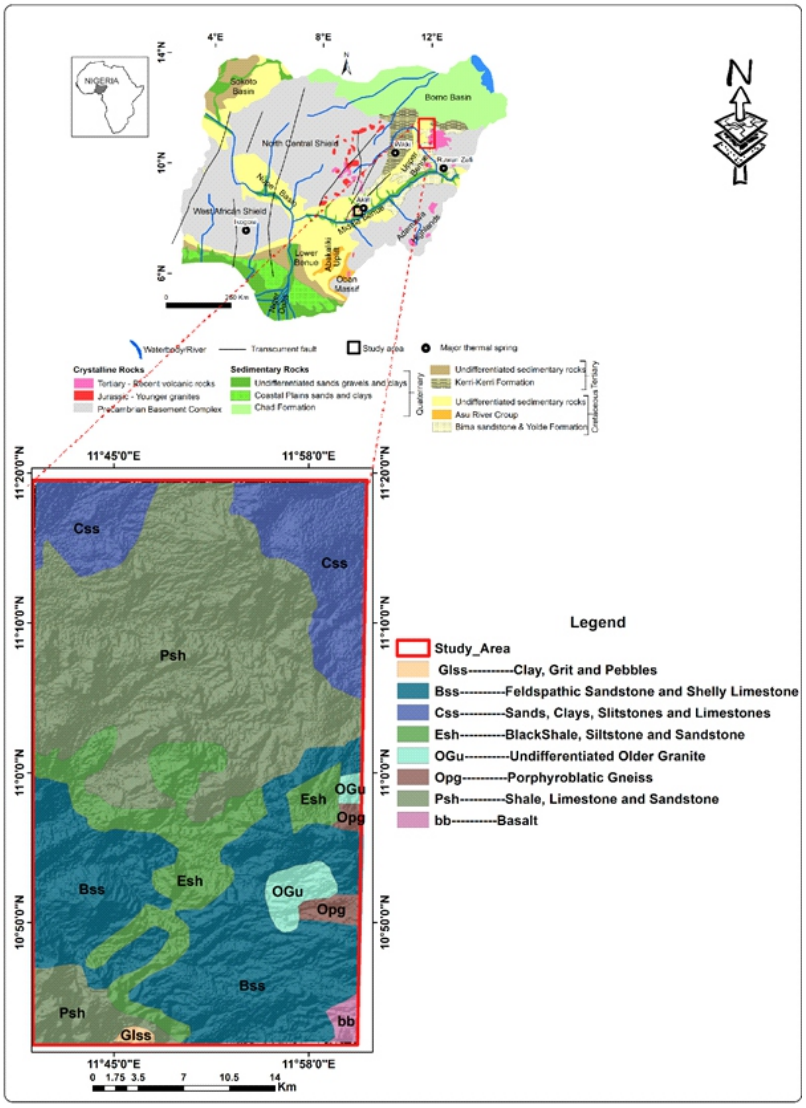

Figure 1: (a) Generalized geological map of Nigeria. (b) Geological map of the study area (modified after Nigerian Geological Survey Agency, 2006) superimposed shaded relief image created from Digital Elevation Model of the study area.

The Upper Benue is characterized by numerous NE-SW trending mylonitic shear zones that were formed during the waning stages of the Pan African Orogeny, which were reactivated as sinistral strike-slip faults during the Cretaceous (Benkhelil, 1989; Guiraud *et al*., 1989). In the Upper Benue, three major northeast-trending fracture zones have been identified: the Gombe fault, the Burashika fault, and the Kwol-Kaltungo lineament. The three major fractures cut across the Cretaceous sediments and impact the basement. The deformation along these fractures is evident as cataclastic and brecciated bands in the basement and crushed sedimentary cover about 100 meters wide (Haruna *et al*., 2012).

MATERIALS AND METHODS

To compare the effectiveness of image enhancement techniques for lithological mapping, the Landsat 8 Operational Land Imager (OLI) data was utilized. The Landsat data (Path 186 and Row 052) and 30 m resolution, and Digital Elevation Model (DEM) acquired by the Shuttle Radar Topographic Mission were downloaded from https://earthexplorer.usgs.gov. The Landsat 8 OLI data consists of eight bands of 30 m resolution between visible and shortwave infrared (Bands 1-7 and 9), one panchromatic band of 15 m resolution (Band 8) and two thermal infrared bands (Bands 10 and 11) of 100 m resolution.

The hillshade of the study area (Figure 1b) was generated from the DEM covering the study area using the hillshade tool available in the Spatial Analyst Toolbox of ArcGIS 10.5. To evaluate lithological discrimination capabilities of Landsat-8 data, five bands (bands 2 to 7) between visible and shortwave infrared were utilized. A false colour composite was first created based on optimum index factor (OIF) (Chavez *et al*., 1980; van der Meer *et al*., 2012). This is calculated for all possible three-band combinations by dividing the sum of standard deviations by the sum of correlations (van der Meer *et al*., 2012). OIF is commonly applied to identify the three bands that contain highest amount of information and the lowest amount duplicated information. The band ratio (BR) technique is one of the oldest image enhancement methods used for lithological discrimination and alteration mapping (van der Meer *et al*., 2012). It is effective in reduction of topographic effects and enhancements of fine differences in the spectral reflectance of rock types (Mahanta and Maiti, 2018; Richards and Jia, 2006; Ghrefat *et al*., 2021; Mohamed et al., 2021). Band ratios are implemented to enhance contrast between surface materials by dividing the reflectance values at peaks and troughs in a spectral reflectance curve (Ibrahim *et al*., 2016). Many forms of BR have been formulated for lithological and alteration mapping, however, the spectral signatures of the dominant lithologies in the area under investigation determine the choice of band ratios (Kusky and Ramadan, 2002; Rezaei *et al*., 2020; Ghrefat *et al*., 2021). For this study, band ratios (4/2, 5/6 and 6/7) were found to be effective. The ratios of Bands 4/2, 5/6 and 6/7 are effective for highlighting areas rich in iron oxide, ferrous and clay minerals respectively (Aisabokhae and Oresajo, 2018). The band ratios were implemented using ENVI 5.3 software and subsequently visualized as FCC.

Multispectral images contain a number of spectral bands (*n*-channels) that are usually correlated. Principal component analysis reduces the dimensionality of image data by transforming highly correlated input bands into new orthogonal principal component axes, thereby creating uncorrelated components that represent most of the important information in the data (Richards and Jia, 2006; Rogge *et al*., 2007; Ibrahim *et al*., 2016). The eigen-vector matrix provides information on the contributions of various input spectral bands to each resulting component. The first component contains the highest amount of variance, and in most cases is influenced by albedo. Principal component analysis was implemented on five bands (bands 2-7) of Landsat 8 data using ENVI 5.3 platform.

Similarly, the Minimum noise fraction (MNF) was implemented on five bands using ENVI 5.3 software. MNF has been extensively applied on multispectral and hyperspectral data to achieve spectral reduction, feature extraction and noise whitening (Kumar *et al*., 2015). The MNF transformation is commonly employed to determine the inherent dimensionality of image data, separate noise in the data, and enhance subsequent processing by reducing the computational requirements (Green *et al*., 1988).

The process compresses the original image bands into new sequential orthogonal components that are ordered according to amount of noise present in the components.

One of the effective ways to utilize the output of image enhancement is through colour enhancement. Colour composite enables utilization of three most important output from these enhancements, which is viewed together in the RGB colour space. Appropriate false colour composites that enable lithologic discrimination were developed from the output of the three image enhancement techniques. They were subsequently fused into a single three-band composite using image fusion technique – (Pohl and van Genderen, 1998). This was done to enable utilization of 9 bands derived from the three enhancement methods since the three data sets were found to provide complementary information. Pixel-based fusion involving colour transformation was used according to Gupta (2018).

RESULTS AND DISCUSSION

By applying different image enhancement methods on Landsat-8 data, the results obtained were interpreted by comparing with existing geological map of the study area. Using OIF, Bands 5, 6 and 7 were found be the most informative with least amount of correlation (Table 1). By comparing the existing geologic map to FCC created by combining these three bands (Figure 2), it is possible to differentiate crystalline rocks (basalts, Older granites and porphyroblastic gneisses, which appear as dark brown in the colour composite, and marked A) from sedimentary rocks (light brown). The sedimentary rocks display very little colour difference with the sequence of feldspathic sandstones and shelly limestone (marked B) appearing as lighter shade of brown than shale, limestone and sandstone. Generally, the FCC offers little information with respect to lithological discrimination.

Table 1: OIF ranking

S/N				OIF Index Highest Ranking
1	b5	b6	b7	(8385.73)
2	b1	b5	b6	(7751.93)
3	b2	b5	b6	(7683.82)
4	b4	b5	b6	(7671.00)
5	b3	b5	b6	(7671.00)
6	b1	b6	b7	(7586.55)

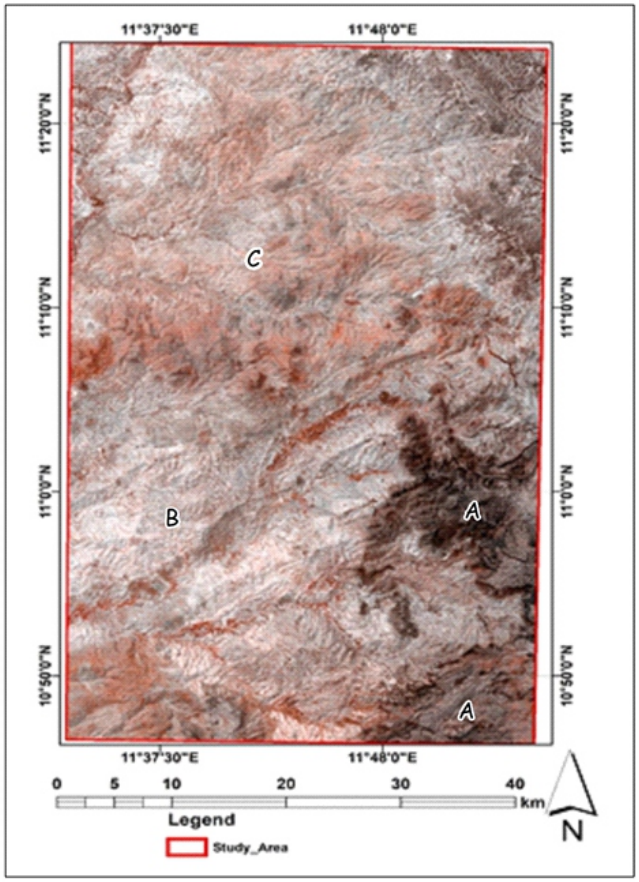

Figure 2: FCC of Band 567 of Landsat-8 of the study area.

Band ratio is designed to enhance the spectral contrast between specific absorption features (Rowan *et al*., 1977; (Rowan *et al*., 2006). The FCC developed from the computed band ratios (4/2, 5/6, 6/7) is presented in Figure 3a. The ratio of bands 4/2 is efficient in the identification for iron oxide minerals (Knepper and Simpson, 1992), while 6/7 is effective for highlighting of OH-bearing clay minerals (Sultan *et al*., 1987; Kaufmann, 1988). By creating FCC of ratio images by inserting 4/2 in Red, 5/6 in Green, and 6/7 in Blue, discrimination between the sedimentary rocks in the area was achieved. On the image, the sequence of feldspathic sandstones and shelly limestones appear reddish (marked B in Figure 3a). Similarly, the sequence of sands, clays, siltstones and limestone display similar reddish colour (marked D in Figure 3a) but with a darker hue. This is indicative of the presence of ferrous oxide minerals in the lithologies (Pour and Hashim, 2012; van der Meer *et al*., 2012). Furthermore, shale, limestone and sandstone (marked C in Figure 3a) appear light blue to purple, while black shale, siltstone and sandstone appear as dark purple (marked E in Figure 3a). This suggests the dominance of hydroxyl-bearing clay minerals in these lithologic units (Sabins 1999; van der Meer *et al*., 2012). Surprisingly, shale, limestone and sandstone in the middle part of the study area (marked H in Figure 3a) appear as a mix of cyan and light green, which is similar to the appearance of crystalline rocks (marked A and G in Figure 3a). The basalts in the study area appear as light green in the FCC, while gneisses and Older Granites display a mix of light green and cyan (marked G in Figure 3a) just like the sequence of shales, limestones and sandstones. The similarity in the spectral signature of gneissic and granitic rocks in enhanced products has been observed in previous studies (Sultan *et al*., 1987; Fagbohun *et al*., 2017; Ghrefat *et al*., 2021). This might be related to the similarity in the mineralogy of the two rock types, which are dominantly composed of feldspar, quartz, and mica.

The variation in colour displayed by the sequence of shale, limestone and sandstone located in the southwestern and central parts of the study area might be associated with variation in mineralogy or texture of the two varieties of this sequence, considering that the spectral characteristics of rocks are dependent on mineralogical composition as well textural characteristics (Hunt, 1977; Clark 1999; Ghrefat *et al*., 2021). Additionally, the proportions of mica and quartz, which are the dominant minerals in shale can vary considerably between two units. Likewise, texture as well as proportion of quartz, feldspar, mica and rock fragments in sandstones can substantially vary. Hence, the spectral signature of sandstones will vary depending on whether they are quartz arenite/wacke, arkosic arenite/wacke, or lithic arenite/wacke. Finally, even though the two units might be composed of shale, limestone and sandstone, the dominant lithology in the units southwestern and central may be different.

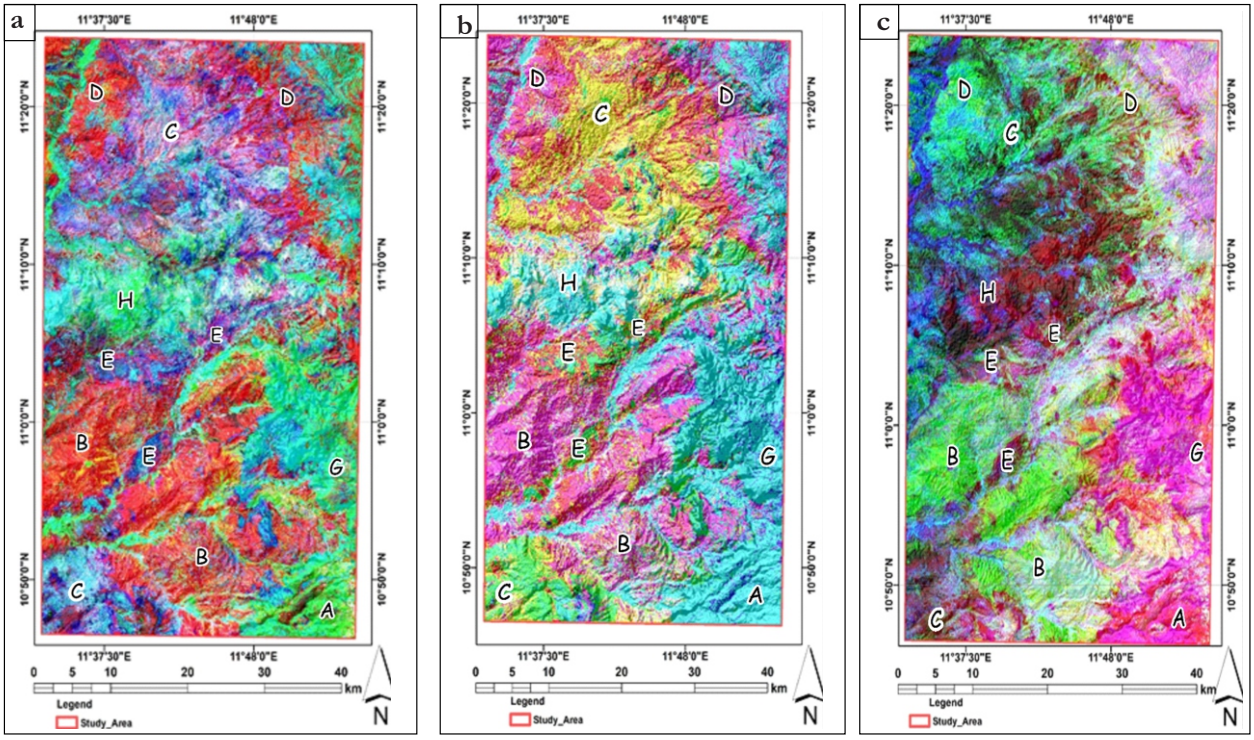

Figure 3: (a) FCC of band ratios 4/2, 5/6 and 6/7 (b) FCC of PC 5, 6 and 7 (c) FCC of MNF 1, 2 and 3.

The FCC derived from PCA and MNF are presented in Figures 3b and 3c, respectively. Comparison of the results shows that PCA is more effective than MNF for lithologic discrimination. Similar to FCC of band ratios, in the FCC developed from the components derived from PCA (PC5, PC6 and PC7) (Figure 3b), both the feldspathic sandstone and shelly limestone (marked B in Figure 3b) and the sequence of sands, clays, siltstone and limestone (marked D in Figure 3b) exhibit similar purplish colour. Nevertheless, the former has a darker shade of purple. By contrast, the sequence of shale, limestone and sandstone (marked C) and the sequence of black shale, siltstone and sandstone (marked E) with similar purplish colour in the BR image (Figure 3a) display disparate colours in some places in the FCC created from PCs (Figure 3b). The former appears as yellow colour in the northern part of the study area, and as light green in the southwestern part of the study area while the latter display a dark green colour (Figure 3b). The similarity in colour displayed by feldspathic sandstone and shelly limestone units (marked B) and sands, clays, siltstone and limestone unit (marked D) in FCCs of BR and PCA might be related to the presence of sand/sandstone and limestone in both sequence. Likewise, the comparable colour displayed by the southern unit of shale, limestone and sandstone (marked C), and black shale, siltstone and sandstone (marked E) in the FCC of PCs, might be also related to the abundance of shale or sandstone in both lithologies resulting in similar reflectance characteristics. Similar to the FCC of BR, the sequence of shale, limestone and sandstone (marked H in Figure 3b) appear as cyan, which is similar to areas where there are crystalline rocks (marked A and G in Figure 3b) although with a slight variation in intensity just as it is observed in the BR image (Figure 3a). The FFC of PCs however does not enable discrimination between the different crystalline rocks in the study area.

The result of MNF offers the least information among the three image enhancing methods. In the FCC created from MNF output (Figure 3c), the sequence of feldspathic sandstone and shelly limestone (marked B) appear as light green. Sands, clays, siltstone and limestone (marked D in Figure 3c) appear as a green while shale, limestone and sandstone (marked C in Figure 3c) also appear as green in the northern part and dark purple in the southern part of the study area. The lithology consisting of shale, limestone and sandstone (marked H in Figure 3c) and the sequence of black shale, siltstone and sandstone (marked E in Figure

3c) both appear as dark purple. Nevertheless, MNF provides optimal distinction between shale, limestone and sandstone (marked H in Figure 3b), which appear as dark purple, and crystalline rocks with the basalt appearing as purplish to reddish (marked A in Figure 3b) and gneiss appearing as magenta (marked in Figure 3b). In both BR and PCA, it is impossible to distinguish shale, limestone and sandstone from crystalline rocks (gneiss and granite).

Considering the three image enhancement methods provide complementary lithological information, it is imperative to combine the three images into a single image to enhance interpretation. The image derived by the fusion of FCCs of band ratios (Figure 3a), principal components (Figure 3b) and minimum noise fraction (Figure 3c) is presented in Figure 4. On the image, most of the lithological units presented in the reference geological can be clearly differentiated. Basalt (marked A) appears as dark blue, gneiss (marked G) appear as dark green, the sequence of shale, limestone and sandstone (marked H) appears as a mix of cyan and blue, the sequence of feldspathic sandstone and shelly limestone (marked B) appear purplish, while sands, clays, siltstone and limestone (marked D) are appear as magenta colour. The sequence of shale, limestone and sandstone (marked C) appear as light green in the southwestern and a mix of yellow and light green in the northern parts of the study area. The sequence of black shale, siltstone and sandstone (marked E) is represented by a mix of green and yellow.

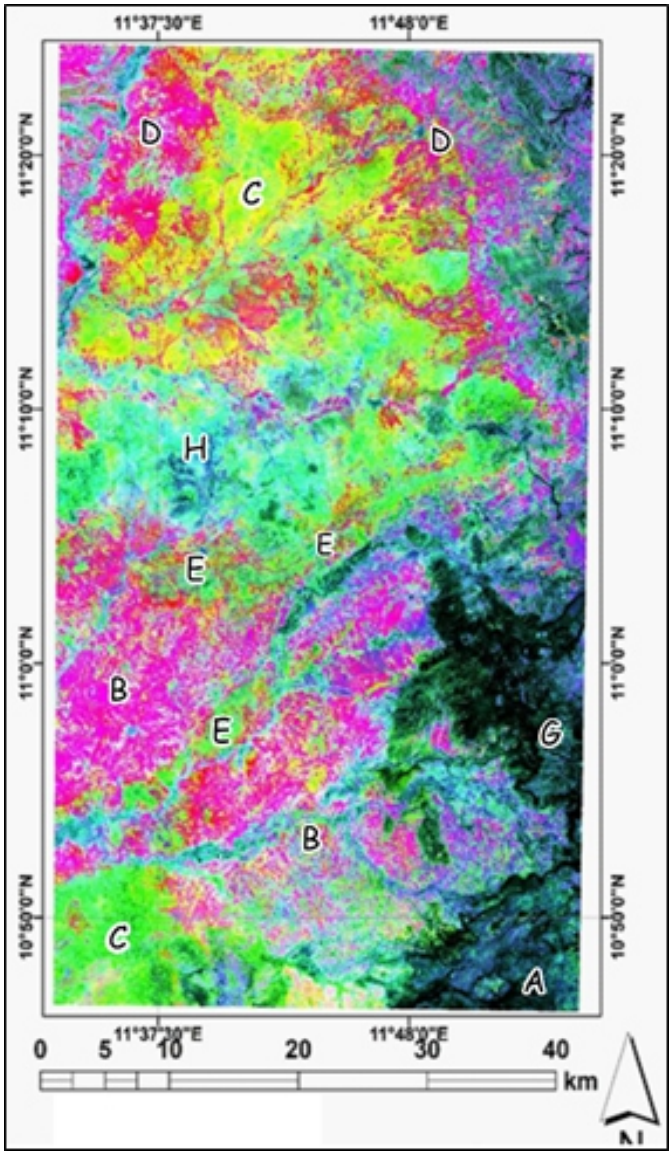

Figure 4: Fused image of BR, MNF and PCA

CONCLUSION

In this study, common image enhancement techniques including OIF, BR, PCA, and MNF were applied on Landsat-8 OLI data. The result obtained showed that BR, PCA, and MNF can be efficiently used for lithological discrimination and mapping in sedimentary terrane. The BR techniques provided the highest amount of information while OIF provided the least amount of information with respect to lithological discrimination. Considering that BR, PCA, and MNF provide complementary information with regards to lithological discrimination, combination of the derivatives from these enhancement methods is necessary to achieve optimal discrimination. This consequently necessitates the fusion of the derivatives from the three methods. Comparison of the patterns present in the fused image with existing geological map, lots of similarities were evident. Nevertheless, it can be observed that some of the lithologic boundaries in the existing map may not be totally accurate. Therefore, the existing geological map of the study area can be improved by reconciliation of existing lithological boundaries with the result of image analysis combined with field visits. The result of this study substantiates the effectiveness of remote sensing as a crucial tool for rapid lithological mapping in areas with no existing geological information or limited geological information. Also, it offers a means to identify areas where detailed field studies need to be focused when the aim is improving of existing geological map.

FUNDING

No funding was received for this research.

DECLARATION OF INTEREST

No conflict of interest among the authors

AUTHORS' CONTRIBUTIONS

Conceptualization: A. O. A., F. B. J., A A. Y. B.
Data gathering and formal analysis: A. O. A.
Writing, review and editing: A. O. A., F. B. J., A.A. Y. B.
Visualization: A. O. A., F. B. J.
Supervision: F. B. J., A.A. Y. B.

REFERENCES

Abdelmalik, K. W. and Abd-Allah, M. A., 2017. Integration of remote sensing technique and field data in geologic mapping of an ophiolitic suture zone in western Arabian Shield. *Journal of African Earth Sciences.* doi: 10.1016/j.jafrearsci.2017.10.006

Abrams, M. J., Brown, D., Lepley, L. and Sadowski, R., 1983. Remote sensing for porphyry copper deposit in southern Arizona. *Economic Geology,* 74(4), 591-604.

Aisabokhae, J., and Oresajo, B., 2018. Application of Remote Sensing Method for Geological Interpretation of Sokoto Plain, Nigeria. *South African Journal of Geomatics*, 7(3), 360-371. doi: 10.4314/sajg.v7i3.12

Benkhelil, J., 1989. The origin and evolution of the Cretaceous Benue Trough (Nigeria). *Journal of African Earth Sciences*, 8, 251-282.

Bentahar, I., and Raji, M., 2021. Comparison of landsat OLI, ASTER, and Sentinel 2A data in lithological mapping : a case study of rich area (central high Atlas, Morocco), *Adv. Space Res.* 67 (3), 945-963. doi: 10.1016/j.asr.2020.10.037.

Burke, K. and Dewey, J. F., 1973. Plume-Generated Triple Junctions: Key Indicators in Applying Plate Tectonics to Old Rocks. *The Journal of Geology,* 81(4), 406-433. doi: 10.1086/627882

Clark, R.N., 1999. Spectroscopy of Rocks and Minerals, and Principles of Spectroscopy. In: Rencz, A.N. (Ed.), Manual of Remote Sensing. John Wiley and Sons, New York, pp. 3-58

Carranza, E. J. M. and Hale, M., 2002. Mineral imaging with Landsat Thematic Mapper data for hydrothermal alteration mapping in heavily vegetated terrane. *International Journal of Geographical Information Science*, 23(22), 4827-4852. doi: 10.1080/01431160110115014

Carter, J. D., Barbar, W. and Tait, E. A., 1963. Geology of parts of Adamawa, Bauchi and Borno Provinces in Northeastern Nigeria. *Geol. Surv. Nig. Bull.*, 30(108).

Chavez, P. S., Berlin, G. L. and Sowers, L. B., (1980). Statistical methods for selecting of Landsat MSS ratios. *Journal of Applied Photographic Engineering*, 8.

Courba, S., Youssef, H., Jamal, A., Abdessalam, O., Mohamed, E., Larbi, B., Assia, I., Zineb, A., Slimane, S., Lahcen, O., Taha, G., Aziza, L., and Ahmed, B. D. M. 2023. Litho-structural and hydrothermal alteration mapping for mineral prospection in the Maider basin of Morocco based on remote sensing and field investigations, *Remote Sensing Applications: Society and Environment*, 31,100980.
doi: 10.1016/j.rsase.2023.100980.

Drury, S. A., 1987. *Image Interpretation in Geology*. First edition, London. Allen and Unwin.

El-din, G. K. and Abdelkareem, M., 2018. Integration of remote sensing, geochemical and field data in the Qena-Safaga shear zone: Implications for structural evolution of the Eastern Desert, Egypt. *Journal of African Earth Sciences*.
doi: 10.1016/j.jafrearsci.2018.02.014

El Janati, M., 2019. Application of remotely sensed ASTER data in detecting alteration hosting Cu, Ag and Au bearing mineralized zones in Taghdout area, Central Anti-Atlas of Morocco. *Journal of African Earth Sciences,* 151, 95-106.
doi: 10.1016/j.jafrearsci.2018.12.002

Fagbohun, B. J., Adeoti, B. and Aladejana, O. O., 2017. Litho-structural analysis of eastern part of Ilesha schist belt, Southwestern Nigeria. *Journal of African Earth Sciences*, 133, 123-137.
doi: 10.1016/j.jafrearsci.2017.05.017

Fahmy, W., El-Desoky, H.M., Elyaseer, M.H., Ayonta Kenne, P., Shirazi, A., Hezarkhani, A., Shirazy, A., El-Awny, H., Abdel-Rahman, A.M., Khalil, A.E., et al. 2023. Remote Sensing, Petrological and Geochemical Data for Lithological Mapping in Wadi Kid, Southeast Sinai, Egypt. *Minerals*, 13, 1160.
doi: 10.3390/min13091160

Gad, S. and Kusky, T., 2002. Lithological mapping in the Eastern Desert of Egypt, the Barramiya area, using Landsat thematic mapper (TM). *Journal of African Earth Sciences*, 44, 196-202.

Ghrefat, H., Kahal, A. Y., Abdelrahman, K., Alfaifi, H. J. and Qaysi, S., 2021. Utilization of multispectral Landsat-8 remote sensing data for lithological mapping of southwestern Saudi Arabia. *Journal of King Saud University - Science*, 33, 101414.
doi: 10.1016/j.jksus.2021.101414

Green, A. A., Berman, M., Switzer, P. and Craig, M. D., 1988. A transformation for ordering multispectral data in terms of image quality with implications for noise removal. *IEEE Transactions on Geoscience and Remote Sensing*, 26(1), 65-74.
doi: 10.1109/36.3001

Guiraud, M., Ajakaiye, D. E. and Ugodulunwa, F. X. O., 1989. Characterisation of late Cretaceous NE-SW sinistral wrench faults in the Upper Benue Trough (Nigeria) using microtectonic and aeromagnetic data. *Journal of African Earth Sciences*, 9(1), 9-21.
doi: 10.1016/0899-5362(89)90003-1

Gupta, R. P., (Ed.). 1981. *Remote Sensing Geology* (Second, Vol. 3). Springer Berlin Heidelberg.

Gupta, R. P., 2018. *Remote Sensing Geology* (Third). Springer-Verlag Berlin Heidelberg.

Hardlar, S. K. 2013. *Mineral Explorations: Principle and Applications*. (S. K. Hardlar, Ed.) (Vol. 2). Elsevier.

Haruna, I. V., Ahmed, H. A. and Ahmed, A. S., 2012. Geology and tectono-sedimentary disposition of the Bima sandstone of the Upper Benue Trough (Nigeria): Implications for sandstone-hosted Uranium deposits. *Journal of Geology and Mining Research*, 4(7), 168-173.
doi: 10.5897/JGMR12.008

Hewson, R., Robson, D., Carlton, A. and Gilmore, P., 2017. Geological application of ASTER remote sensing within sparsely outcropping terrain, Central New South Wales, Australia. *Cogent Geoscience*, 3(1), 1-22.
doi: 10.1080/23312041.2017.1319259

Hunt, G.R., 1977. Spectral signatures of particulate minerals in the visible and near infrared. *Geophys*. 42 (3), 501-513.

Ibrahim, W. S., Watanabe, K. and Yonezu, K., 2016. Structural and litho-tectonic controls on Neoproterozoic base metal sulfide and gold mineralization in North Hamisana shear zone, South Eastern Desert, Egypt: The integrated field, structural, Landsat-7 ETM+ and ASTER data approach. *Ore Geology Reviews*, 79, 62-77.

Idi, B. Y., and Aliyu, M., 2015. Mineralogical mapping of the upper Benue Trough Northeastern Nigeria from multispectral remotely sensed data using Linear Spectral Unmixing. "2015 IEEE International Geoscience and Remote Sensing Symposium (IGARSS), Milan, Italy. 3419-3421.
doi: 10.1109/IGARSS.2015.7326554

Isiorho, S. A., 1989. Geologic Remote Sensing in The Upper Benue Trough of Nigeria. "12 Canadian Symposium on Remote Sensing Geoscience and Remote Sensing Symposium, Vancouver, BC, Canada, pp 1430-1433.
doi: 10.1109/IGARSS.1989.576157

Kaufmann, H., 1988. Mineral exploration along the Aqaba-Levent structure by use of Landsat TM data; concepts, processing, and results. *International. Journal of Remote Sensing*, 9(1639), 624 1658.

Knepper, Jr., D. H. and Simpson, S. L., 1992. Remote Sensing in U.S Geological Survey; Bing Bend area; MarfaMH13-5, Fort Stockton MH 13-6, Presidio MH 13-8, Emory Peak MH 13-9: US Department of Energy Open-File Report GJBX-88-79, 5 volumes

Kumar, C., Shetty, A., Raval, S., Sharma, R. and Ray, P. K. C., 2015. Lithological Discrimination and Mapping using ASTER SWIR Data in the Udaipur area of Rajasthan, India. P*rocedia Earth and Planetary Science*, 11, 180-188.
doi: 10.1016/j.proeps.2015.06.022

Kusky, T. M. and Ramadan, T. M., 2002. Structural controls in the Neoproterozoic Allaqi suture: an integrated field, Landsat TM, and radar C/X SIR SAR images. J. Afr. Earth Sci. 35, 107-121.

Lopes, F. C., Pereira, A. J., Mantas, V. M. and Mpengo, H. K., 2016. Morphostructural characterization of the western edge of the huila plateau (SW Angola), based on remote sensing techniques Fernando. *Journal of African Earth Sciences*, 117, 114-123.
doi: 10.1016/j.jafrearsci.2016.01.007

Mahanta, P. and Maiti, S., 2018. Regional scale demarcation of alteration zone using ASTER imageries in South Purulia Shear Zone, East India: Implication for mineral exploration in vegetated regions. *Ore Geology Reviews,* 102, 846-861.
doi: 10.1016/j.oregeorev.2018.07.028

Mohamed, M. T. A., Al-Naimi, L. S., Mgbeojedo, T. I. and Agoha, C. C., 2021. Geological mapping and mineral prospectivity using remote sensing and GIS in parts of Hamissana, Northeast Sudan. *Journal of Petroleum Exploration and Production* 11:1123-1138.
doi: 10.1007/s13202-021-01115-3

Nigerian Geological Survey Agency, 2006. Geological Map of Nigeria.

Ofoegbu, C. O., 1985. A review of the geology of the Benue Trough, Nigeria. *Journal of African Earth Sciences*, 3(3), 283-291.

Okereke, C. N., Onu, N. N., Ibe, K. K., Sele,o, A. O. I., Opara, A. I., Ikoro, D. O., Ibeneme, S. I., and Oha, I. A., 2012. Analysis of Landsat and Aeromagnetic Data for Mapping Linear Structures: A Case Study of Yola Area, Upper Benue Trough, Nigeria. *International Journal of Engineering Research and Applications*, 2(3), pp 1968-1977.

Olade, M. A., 1975. Evolution of Nigeria's Benue Trough (Aulacogen): a tectonic model. *Geol. Mag.*, 122, 575-581.

Onum, A. S., Ibeneme, S. I., Okereke, C. N., Okenu, Y. E., and Uche, S. C. I., 2021. Integration of Landsat Imagery and High Resolution Aeromagnetic Data for Hydrothermal Alteration Mapping in Parts of the Middle Benue Trough

Peyghambari, S., Zhang, Y., 2021. Hyperspectral remote sensing in lithological mapping, mineral exploration, and environmental geology: an updated review. *J. Appl. Remote Sens*. 15 (3).
doi: 10.1117/1.JRS.15.031501

Pohl, C. and van Genderen, J. L., 1998. Multisensor image fusion in remote sensing: concepts, methods and application. *Int J Remote Sens,* 19, 823-854.

Pour, A. B. and Hashim, M., 2012. The application of ASTER remote sensing data to porphyry copper and epithermal gold deposits. *Ore geology reviews*, 44, 1-9.

Pour, A. B., Hashim, M., Hong, J. K. and Park, Y., 2017. Lithological and alteration mineral mapping in poorly exposed lithologies using Landsat-8 and ASTER satellite data: north-eastern Graham Land, Antarctic Peninsula. *Ore Geology Reviews.*
doi: 10.1016/j.oregeorev.2017.07.018

Pour, B. A. and Hashim, M., 2013. Fusing ASTER, ALI and Hyperion data for enhanced mineral mapping. International Journal of Image and Data Fusion, 4, 126-145.

Rajendran, S., Hersi, O. S., Al-harthy, A., Al-wardi, M., El-ghali, M. A., and Al-abri, A. H., 2011. Capability of advanced spaceborne thermal emission and reflection radiometer (ASTER) on discrimination of carbonates and associated rocks and mineral identification of eastern mountain region (Saih Hatat window) of Sultanate of Oman. *Carbonates Evaporites*, 26, 351-364.
doi: 10.1007/s13146-011-0071-4

Rezaei, A., Hassani, H., Moarefvand, P. and Golmohammadi, H., 2020. Lithological mapping in Sangan region in Northeast Iran using ASTER satellite data and image processing methods. *Geology, Ecology, and Landscapes*, 4(1), 59-70.
doi: 10.1080/24749508.2019.1585657

Richards, J. A., and Jia, X., 2006. *Remote sensing digital image analysis* (Forth). Springer.

Rogge, D. M., Rivard, B., Zhang, J., Sanchez, A., Harris, J. and Feng, J., 2007. Integration of spatial - spectral information for the improved extraction of end members. *Remote Sensing of Environment*, 110, 287-303.
doi: 10.1016/j.rse.2007.02.019

Rowan, L. C., Goetz, A. F. H. and Ashley, R. P., 1977. Discrimination of hydrothermally altered and unaltered rocks in visible and near-infrared multispectral images. *Geophysics*, 42, 522-535.

Rowan, L. C., Schmidt, R. G. and Mars, J. C., 2006. Distribution of hydrothermally altered rocks in the Reko Diq, Pakistan, mineralized area based on spectral analysis of ASTER data. *Remote Sensing of Environment*, 104, 74-87.

Sabins, F. F., 1999. Remote sensing for mineral exploration. *Ore Geology Reviews*, 14, 157-183.

Suliman, M., Ali, M., & Faisal, S., 2023. Lithological mapping of the northern Kohat Plateau's limestone outcrop using integrated remote sensing and reflectance spectroscopy technique. *Geology, Ecology and Landsacpes.*
doi: 10.1080/24749508.2023.2256550

Sultan, M., Arvidson, R. E. and Sturchio, N. C., 1986. Mapping of serpentinites in the Eastern Desert of Egypt using Landsat Thematic Mapper data. *Geology*, 14, 995-999.

Sultan, M., Arvidson, R. E., Sturchio, N. C., and Guinness, E. A., 1987. Lithological mapping in arid regions with Landsat thematic mapper data: Meatiq dome, Egypt

van der Meer, F. D., van der Werff, H. M., van Ruitenbeek, F. J., Hecker, C., Bakker, W. H., Noomen, M. F., Woldai, T., 2012. Multi- and hyperspectral geologic remote sensing: A review. *International Journal of Applied Earth Observation and Geoinformation,* 14(1), 112-128.
doi: 10.1016/j.jag.2011.08.002

Wright, J. B., 1985. *Geology and mineral resources of West Africa*. (J. B. Wright, Ed.). George Allen & Unwin (Publishers) Ltd, 40 Museum Street, London WCIA lLU, UK George.

Xi, Y., Mohamed Taha, A.M., Hu, A., and Liu, X. 2022 Accuracy comparison of various remote sensing data in lithological classification based on random forest algorithm. *Geocarto Int.* 37 (26) 14451-14479,
doi: 10.1080/10106049.2022.2088859.

Zoheir, B., Emam, A., El-wahed, M. A. and Soliman, N., 2019. Gold endowment in the evolution of the Allaqi-Heiani suture, Egypt: A synthesis of geological, structural, and space-borne imagery data. *Ore Geology Reviews*, 102938.
doi: 10.1016/j.oregeorev.2019.102938